Available online at www.sciencedirect.com

ScienceDirect

journal homepage: www.elsevier.com/locate/he

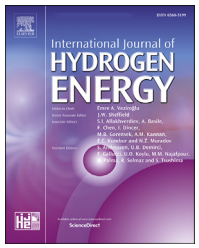

Short Communication

Carbon-coated cobalt molybdenum oxide as a high-performance electrocatalyst for hydrogen evolution reaction

Ning Xu [a], *Guoxuan Cao* [a], *Liyong Gan* [a], *Zhengjun Chen* [a], *Mingjie Zang* [a], *Hui Wu* [b], *Ping Wang* [a,*]

[a] *School of Materials Science and Engineering, South China University of Technology, Guangzhou 510641, PR China*
[b] *NIST Center for Neutron Research, National Institute of Standards and Technology, Gaithersburg, MD 20899-6102, United States*

ARTICLE INFO

Article history:
Received 12 July 2018
Received in revised form
25 October 2018
Accepted 28 October 2018
Available online 22 November 2018

Keywords:
Water-splitting
Hydrogen evolution reaction
Cobalt molybdenum oxide
Hydroxide nanoplates

ABSTRACT

Synthesis of high-performance and cost-effective catalysts towards the hydrogen evolution reaction (HER) is critical in developing electrochemical water-splitting as a viable energy conversion technique. For non-precious metal Co- and Ni-based catalysts, hydroxides were found to form on the surface of the catalysts under alkaline environments and benefit the catalytic performance, whereas there is limited systematic study on the explicit influence of hydroxides on the electrocatalytic mechanism and performance of these catalysts. Herein, we report a close correlation observed between the amount of the surface hydroxides formed and the resulting electrocatalytic performance of a Co-Mo-O nanocatalyst through careful comprehensive structural and property characterizations. We found that an appropriate amount of hydroxide can be moderated by simply coating the catalyst surface with carbon shells to optimize the catalytic properties. As a result, a carbon-coated Co-Mo-O nanocatalyst was successfully developed and is among the best reported non-precious HER catalysts with a superior electrocatalytic activity and outstanding durability for the HER under alkaline environment. First-principles calculations were further conducted to probe the nature of the active sites and the role of hydroxides in the Co-Mo-O@C/NF catalyst towards the HER.

Introduction

The widespread utilization of clean renewable energy resources is increasingly being pursued as a solution to the world's energy, climate and environmental problems. Due to the intermittent nature of energy generation from renewable sources such as solar and wind energy, it is urgently required to develop viable energy conversion technologies to enable the decoupling of energy generation from demand. In this

* *Corresponding author.*
E-mail address: mspwang@scut.edu.cn (P. Wang).
https://doi.org/10.1016/j.ijhydene.2018.10.201

respect, electrochemical water-splitting provides a promising energy conversion technology that converts electrical energy into chemical energy in the form of H_2, an attractive energy carrier that can be used to produce clean electricity in fuel cells. Crucial to enabling this conversion is the development of high-performance electrocatalysts for the hydrogen evolution reaction (HER) and oxygen evolution reaction (OER) reactions [1–6].

The best-performing catalyst for the HER thus far is platinum, which requires negligible overpotentials to achieve high electrocatalytic performance. However, its widespread use in electrolysis of water is limited by its scarcity and high cost [7,8]. Hence, a variety of non-precious metal alloys, such as transition metal sulfides [9–12], phosphides [13,14], carbides [15–17], nitrides [18,19], selenides [20–22], oxides [23–25], borides [26–28] and non-metallic compound [29,30] have been investigated as promising alternatives to replace Pt. In addition, non-precious metal complexes also emerged as promising homogeneous catalysts for the HER. In comparison with the homogenous molecular catalysts, heterogeneous catalysts typically show much lower catalytic efficiency owing to the low ratio of surface to bulk atoms. But on the other hand, heterogeneous catalysts possess notable advantages over the homogeneous catalysts on easy synthesis, facile separation and cyclic reusability [14,31–33]. Therefore, high-performance and cost-effective heterogeneous catalysts are desirable for practical applications. In practice, the activity of these non-precious catalysts can be promoted through increasing the number of the active sites, primarily via nanostructuring the electrocatalytic materials, and improving the intrinsic activity of each active site. These two approaches are often jointly adopted to optimize the catalytic performance of catalysts [34]. This is evident from the encouraging progresses in developing nanostructured bimetallic HER catalysts, like the "state-of-the-art" Co-Mo-S, Ni-Mo-N catalysts [35–40].

Electrocatalytic reaction involves unidirectional electron-transferring between the electrode and reactants. Therefore, electrical conductivity is a key factor in influencing the catalytic performance of these non-Pt electrocatalysts. However, compared to the intense studies on the intrinsic activity as well as the number and the accessibility of active sites of the bimetallic HER electrocatalysts, the electrical conductivity of these electrocatalysts received limited attention. For the Co- and Ni-based catalysts our latest study found that their electrical conductivity might be closely related to the surface oxidation states of the catalysts. It has been experimentally found that hydroxide or oxide nanoplates will form on the surface of Co- and Ni-based catalysts under alkaline environments even in the HER potential region [41–43]. The resulting hydroxide or oxide was proposed to work in concert with the adjacent metal atoms to form active sites, where the hydroxide or oxide promotes the dissociation of water and the nearby metal atoms facilitate the adsorption and association of hydrogen intermediates into molecular H_2 [34,44]. But on the other hand, the flourishing growth of hydroxide or oxide nanoplates may deteriorate the electrocatalytic performance due to their low electrical conductivity. This detrimental effect will become dominant once the catalyst surface is completely covered by the hydroxide or oxide layer and separated from the conductive substrate. More recently, we found that this problem can be circumvented by simply coating the catalyst with carbon shells. Here, it should be noted that coating an irregular surface with a coherent carbon shell of uniform thickness is technically extremely difficult [45,46]. In our study, we intentionally utilized the nonuniformity of carbon shell to regulate the growth of hydroxide nanoplates. This is substantially different from the strategy used in the previous literature, which requires a carefully controlled synthesis of ultrathin graphene shells to render electron penetration from the CoNi core to the graphene surface [47]. The new method is widely adaptable to various nanostructured metal electrocatalysts and can readily be scaled up for mass production. In particular, it provides a simple but effective approach to simultaneously addressing the electrical conductivity and the active site issues of noble-free HER catalysts operated under alkaline environments.

Herein, we synthesize a carbon-coated cobalt molybdenum oxide nanocatalyst supported on nickel foam (denoted as Co-Mo-O@C/NF) using a simple hydrothermal method (see the Experimental Section for details). Associated with the regulated growth of hydroxide nanoplates by carbon shells, the Co-Mo-O@C/NF catalyst exhibits excellent HER activity along with outstanding stability in alkaline solutions, outperforming most non-precious metal electrocatalysts.

Experimental section

Electrode preparation

The Co-Mo-O@C electrocatalyst was in situ grown on NF using a hydrothermal method followed by calcination treatment. The NF was consecutively cleaned in HCl solution (3 M), ethanol and DI water under sonication to remove nickel oxides, organics and other impurities on the surface. $Co(NO_3)_2 \cdot 6H_2O$ (0.05 M), urea (0.25 M), glucose (0.08 M) and $(NH_4)_6Mo_7O_{24} \cdot 4H_2O$ (0.025 M) were dissolved in 36 mL DI water, and then the solution together with a cleaned piece of NF (1 × 4 cm^2) were transferred into a 50 mL Teflon-lined stainless autoclave and kept at 150 °C for 18 h. After cooling down to room temperature, the collected samples were washed thoroughly with DI water and ethanol and then dried in vacuum at 60 °C. Calcination of the catalyst samples was conducted at temperatures ranging from 400 to 800 °C under a flowing H_2 atmosphere for 2 h with a ramp rate of 10 °C min^{-1}. Electrochemical property testing showed that the Co:Mo molar ratio and calcination treatment temperature exerted considerable effects on the HER activity of Co-Mo-O@C/NF catalyst. According to the control experiments (Fig. S2a and b), the 600 °C calcined Co-Mo-O@C/NF catalyst with a nominal Co:Mo molar ratio of 1:3.5 exhibited an optimal HER activity. It was therefore selected for detailed study. As determined by inductively coupled plasma-atomic emission spectrometry (ICP-AES), the optimized catalyst has an authentic Co: Mo molar ratio of 1: 1.2. According to the weight change of the sample after hydrothermal and calcination processes, the loading amount of the catalyst on NF was determined to be around 8 mg cm^{-2}. For comparison purpose, the supported Co@C/NF catalyst was also prepared in a similar

procedure without using $(NH_4)_6Mo_7O_{24}\cdot 4H_2O$ in the hydrothermal step.

The Co-Mo-O/NF electrocatalyst was prepared by electrochemical oxidation of the Co-Mo-O@C/NF catalyst followed by calcination treatment. The electrochemical oxidation of Co-Mo-O@C/NF catalyst was carried out in a standard three-electrode system using an Hg/HgO (with 1M KOH) reference electrode and graphite rod as the counter electrode in an alkaline medium (1M KOH). After electrochemical oxidation under 1.4 V (vs. RHE) for 10 min, the catalyst was thoroughly washed by DI water and ethanol, then dried in oven at 60 °C. Calcination treatment of the catalyst was conducted at 600 °C under a flowing H_2 atmosphere for 2 h. The ramping rate was 10 °C min^{-1}.

Results and discussion

Morphology observation of the Co-Mo-O@C/NF sample by field-emission scanning electron microscopy (FE-SEM, Fig. 1a and b) showed that the surface of NF was entirely covered by bundles of rectangular cuboids, which self-assembled into 3D hierarchical network structure. The width and length of rectangular cuboids were around 2 μm and 10–30 μm, respectively. In addition, some nanoparticles in different aggregation states were observed on the surface of these rectangular cuboids, which were identified as carbon-rich particles by the elemental mapping analyses (Fig. S1). X-ray diffraction (XRD) analysis of the as-prepared catalyst clearly identified two crystalline phases, i.e., $Co_2Mo_3O_8$ (JCPDS card 71-1423) and Co_3Mo (JCPDS card 29-0488), as shown in Fig. 2a. This aligns with the high-resolution transmission electron microscopy (HRTEM, Fig. 1e) image, in which the observed lattice fringes with spacings of 0.349 and 0.4957 nm correspond well to the (102) and (002) planes of $Co_2Mo_3O_8$, and those with distances of 0.349 and 0.4957 nm in a characteristic angle of 25.3° can be accounted by the (200) and (201) planes of Co_3Mo alloy. A close examination of the catalyst sample by HRTEM clearly showed that the surface of the rectangular cuboids was coated by carbon shells with varied thicknesses. As shown in the representative images in Fig. 1e, the numbers of graphene layers ranged from one to ten. In accordance with the HRTEM results, Raman spectroscopy analysis of the sample identified the distinct characteristic G and D bands of carbon materials at 1590 and 1360 cm^{-1}, respectively (Fig. 2b).

The Co-Mo-O@C/NF catalyst exhibited a small but significant morphology change after the electrochemical activation. FE-SEM (Fig. 1c) showed that some tiny hexagonal plaques grow upright and stab perpendicularly to the surface of the Co-Mo-O@C rectangular cuboids. The average size and thickness of these nanoplates were around 130 and 30 nm, respectively. An HRTEM image (Fig. 1g) on the activated Co-Mo-O@C catalyst illustrated the polycrystalline nature of the nanoplates, as shown by a series of concentric diffraction rings in the selected area electron diffraction (SAED) pattern (inset in Fig. 1g), which can be matched by the corresponding

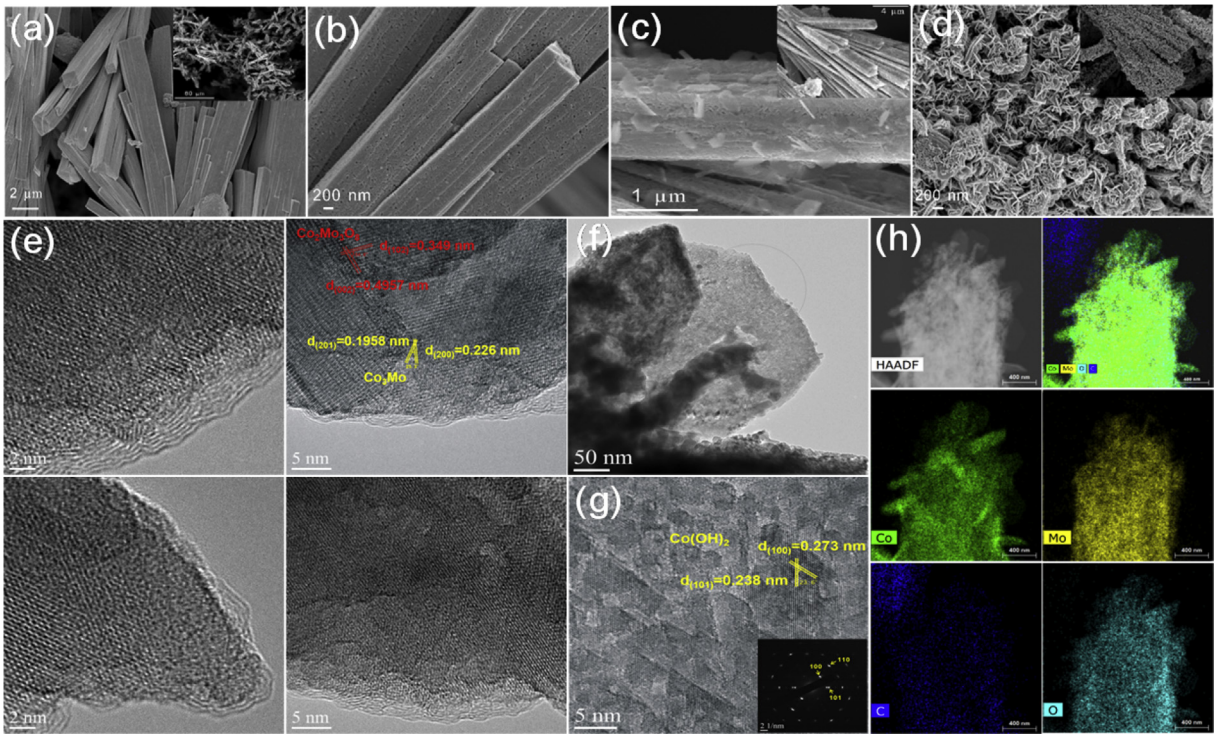

Fig. 1 – a) and b) FE-SEM images of Co-Mo-O@C/NF at different resolutions. c) and d) FE-SEM images of the post-HER Co-Mo-O@C/NF and Co-Mo-O/NF catalysts, respectively. The insets show the corresponding low-magnification SEM images. e) HRTEM images of Co-Mo-O@C. f) TEM image of the post-HER Co-Mo-O@C. g) HRTEM image of the post-HER Co-Mo-O@C, the inset shows the corresponding SAED pattern. h) HAADF-STEM image of the post-HER Co-Mo-O@C sample and corresponding EDS mapping results for Co, Mo, C, O and combined image, respectively.

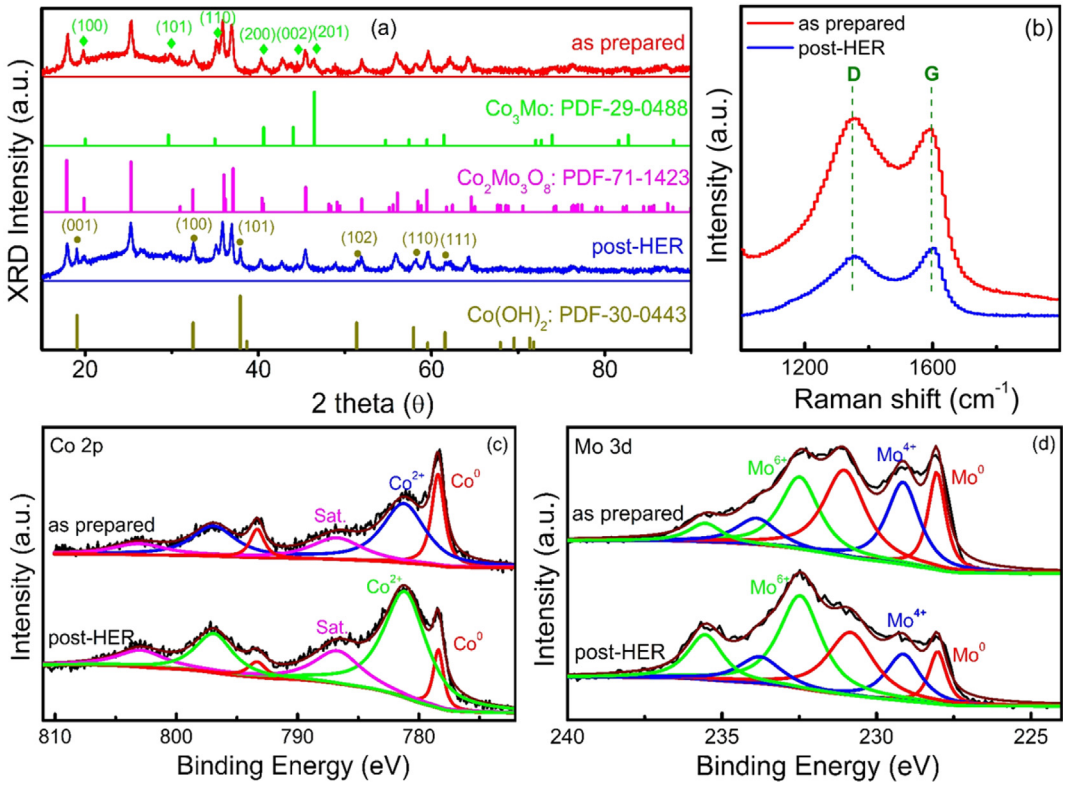

Fig. 2 – a) and b) XRD patterns and Raman spectra of the as-prepared and post-HER Co-Mo-O@C powders, respectively. XPS spectra of the as-prepared and post-HER Co-Mo O@C/NF catalysts in the c) Co 2p and d) Mo 3d regions.

crystalline planes of β-$Co(OH)_2$. Consistently, the lattice fringes with interplanar distances of 0.238 and 0.273 nm can be assigned to (101) and (100) crystalline planes of β-$Co(OH)_2$. The XRD result (Fig. 2a) further the formation of β-$Co(OH)_2$ (JCPDS card 30-0443) and the retainment of $Co_2Mo_3O_8$ phase after electrochemical activation. The high-angle annular dark-field scanning transmission electron microscopy (HAADF-STEM) mode combining with energy dispersive X-ray spectroscopy (EDS) analysis discerned that the nanoplates growing during the HER from the Co-Mo-O substrate were free of Mo elements.

The X-ray photoelectron spectroscopy (XPS) was employed to characterize the chemical state and constituent elements on the catalyst surface. As shown in Fig. 2c, the Co 2p spectra of the as-prepared and activated Co-Mo-O@C/NF catalysts can be fitted with two doublets assigned to metallic Co^0, Co^{2+} and satellite features. The Co^0 signal detected in the as-prepared Co-Mo-O@C/NF catalyst is consistent with the observation of Co_3Mo alloy in the XRD analysis. The XPS after the electrochemical activation of the catalyst showed a weakened signal of metallic Co^0, which was accompanied with the strengthening of the Co^{2+} signal. These results were in good agreement with the formation of β-$Co(OH)_2$ in the electrochemically active sample as evidenced by the XRD and HRTEM results. Similarly, the Mo 3d spectra can be resolved well with the signals of metallic Mo^0, Mo^{4+} and Mo^{6+} (Fig. 2d). The lessened intensity of the metallic Mo^0 signal relative to oxide species in the activated sample might be attributed to surface oxidation in the alkaline solution and/or air exposure. Similar phenomena have been reported for CoMo-based HER catalysts [48].

Fig. 3a presented the polarization curves of the as-prepared Co-Mo-O@C/NF, Co-Mo-O/NF, Co@C/NF, bare NF along with the commercial Pt/C (20 wt%) for reference (the preparation and nomenclature of Co-Mo-O/NF and Co@C/NF can be found in the experimental section in supporting information). It was observed that the Co-Mo-O@C/NF catalyst required only 20 mV overpotential to reach a current density of 10 mA cm^{-2} in 1 M KOH solution, which is comparable to the benchmark Pt/C catalyst and among the best reported levels for noble-free HER catalysts (Table S1). In order to provide further insight into variation of HER activities on the series of electrocatalysts, the electrochemical impedance spectroscopy (EIS) technique was employed to measure the charge transfer resistance (R_{ct}), as well as the electrical double-layer capacitance (C_{dl}) to determine the electrochemically active surface area (ECSA). As seen in Fig. 3b and c, incorporation of Mo into the catalyst improves electrical process, while coating the catalyst surface with carbon shells enhances both electrical conductivity and ECSA. Here, it should be noted that the Co-Mo-O/NF catalyst was prepared by controlled electrooxidation of Co-Mo-O@C/NF catalyst followed by calcination treatment under H_2 atmosphere (Fig. S3). Directly synthesized Co-Mo-O/NF catalyst by hydrothermal method may differ substantially from the conductivity, which makes it difficult to evaluate the effect of carbon shells on the catalyst surface. To better understand the role of carbon shells in the electrocatalysis process, we further compared the Co-Mo-O@C/NF

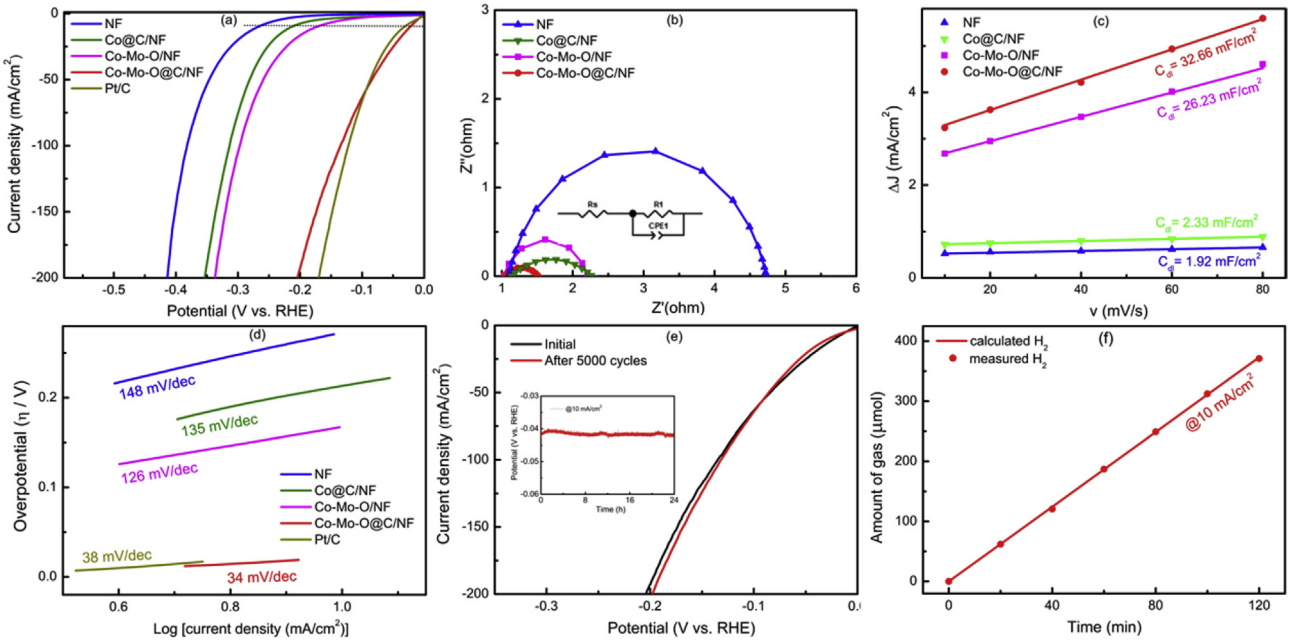

Fig. 3 – a) HER polarization curves. b) Electrochemical impedance spectroscopy (EIS) analyses of the electrocatalysts. c) The capacitive current densities at open circuit potential (OCP) as a function of scan rate. d) The corresponding Tafel plots of the electrocatalysts. e) The polarization curves of the Co-Mo-O@C/NF with a scan rate of 100 mV s^{-1} before and after 5000 cycles. The inset shows the chrono potentiometric curve at 10 mA cm^{-2}. f) The amount of gas experimentally measured and theoretically calculated *versus* time for HER of the Co-Mo-O@C/NF under constant current density of 10 mA cm^{-2}.

and Co-Mo-O/NF catalysts in terms of morphological feature and electrical conductivity. Morphological observations (Fig. 1d) in combination with microstructure analyses by HRTEM and SAED (Fig. S4) showed that the surface of the post-HER Co-Mo-O/NF catalyst was entirely covered by voluminous irregularly shaped β-$Co(OH)_2$ nanoplates, which is in sharp contrast to the morphological feature of the activated Co-Mo-O@C/NF sample (Fig. 1c) with only scattered tiny hexagonal flakes of β-$Co(OH)_2$ on the surface. The EIS measurements (Fig. S5) revealed that the Co-Mo-O/NF catalyst exhibited notable increase of R_{ct} after electrochemical activation (from 33.68 to 89.31Ω), whereas the Co-Mo-O@C/NF sample showed only a slight R_{ct} increase. It is evident that the stacking of large amounts of low-conductive nanoplates on the catalyst surface resulted in significantly degraded electrical conductivity of the Co-Mo-O/NF catalyst. A combined analysis of these results suggests that the formation of $Co(OH)_2$ nanoplates on the catalyst surface is closely correlated to the electrical conductivity and the catalytic activity of the catalyst (Table S2). Therefore, properly regulating the formation of $Co(OH)_2$ nanoplates by carbon shells on the catalyst surface may provide a viable means to achieve an optimization between the number of active sites and the electrical conductivity of the electrocatalysts.

Tafel analysis of the polarization curves was conducted to perceive the mechanism of the HER. As seen in Fig. 3d, the Tafel slopes of the Co-Mo-O/NF and Co@C/NF catalysts were determined to be 126 and 135 mV dec^{-1}, respectively, while the Co-Mo-O@C/NF catalyst showed a distinctively small Tafel slope of only 34 mV dec^{-1}, suggesting that the initial electron-transfer step through the discharge of water (Volmer step) is the rate-determining step [19,49]. First-principles calculations were then modelled based on the experimental observations and performed to rationalize these phenomena. Specifically, the elementary reactions associated with water dissociation (Volmer step) and the subsequent formation of molecular H_2 (Tafel or Heyrovsky step) were investigated on the Co_3Mo

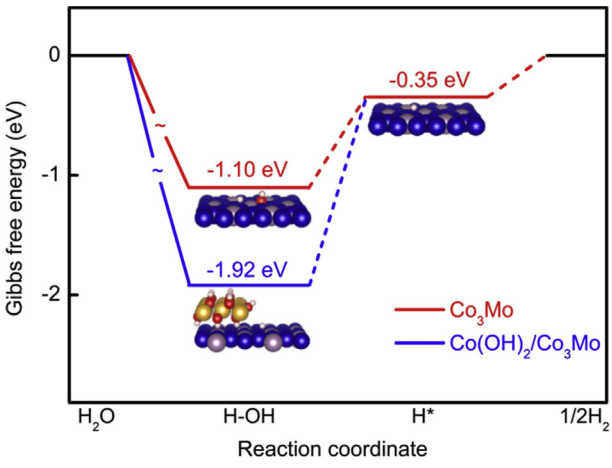

Fig. 4 – Gibbs free energy diagram for the HER on the Co_3Mo surface (red) and $Co(OH)_2/Co_3Mo$ interface (blue). Insets show the optimized structures at different reaction stages. The blue, gold, red and white balls represent Co, Mo, O and H atoms, respectively. (For interpretation of the references to color in this figure legend, the reader is referred to the Web version of this article.)

surface and the $Co(OH)_2/Co_3Mo$ interface (Fig. S6) [50,51]. Fig. 4 shows the Gibbs free energy diagram for the two sequential steps on the two modelled substrates with optimized structures. The calculated Gibbs free energy change of water dissociation, $\Delta G(H_2O)$, on the $Co(OH)_2/Co_3Mo$ interface is much larger than that on the Co_3Mo surface (−1.92 vs. −1.10 eV), highlighting the critical beneficial role of the interfacial $Co(OH)_2$ in promoting the dissociative adsorption of water. The resulting H intermediates from water dissociation can readily be converted into molecular H_2 on the Co_3Mo surface with a calculated $\Delta G(H^*)$ of only −0.35 eV [52–55]. These calculation results clearly suggested that $Co(OH)_2$ may work cooperation with Co_3Mo to properly address different elementary steps, thereby the resulting $Co(OH)_2/Co_3Mo$ interfaces from the electrochemical activation may give highly active site for the HER.

Long-term stability is also an important criterion for assessing the HER catalysts. The chronopotentiometry and cyclic voltammetry (CV) methods were employed to test the durability of Co-Mo-O@C/NF catalyst. As shown in Fig. 3e, the Co-Mo-O@C/NF catalyst showed an overpotential fluctuation of only 2 mV in a 24 h of constant-current measurement at 10 mA cm^{-2}, and the activity was even slightly improved after 5000 CV cycles. As present in Fig. S7, the SEM morphology observations showed that the morphological feature of the long-term operation catalyst was well retained. It was clearly observed that the outstanding durability of the Co-Mo-O@C/NF catalyst for the HER in alkaline solutions. The Faradic efficiency (FE) for HER process was evaluated by comparing the amount of experimentally determined gas with theoretical values. As shown in Fig. 3f, the collected H_2 amounts perfectly matched the calculated values based on passed charge, leading to a nearly 100% FE of the Co-Mo-O@C/NF catalyst for the HER.

Conclusions

In summary, a carbon-coated Co-Mo-O nanocatalyst supported on nickel foam (Co-Mo-O@C/NF) was synthesized with a simple hydrothermal method followed by a calcination process under H_2 atmosphere. The Co-Mo-O@C/NF catalyst exhibited superior electrocatalytic activity and outstanding durability for the HER under alkaline environment, which is among the best reported noble-free HER catalysts. Our study found that the formation of $Co(OH)_2$ nanoplates on the catalyst surface is closely correlated to the electrical conductivity as well as the catalytic activity of Co-based HER catalyst. Coating the catalyst surface with carbon shells has been proved as a simple but effective approach to moderating the growth of $Co(OH)_2$ nanoplates so as to attain high and stable catalytic activity. This method might be widely adoptable in the development of high-performance non-precious electrocatalytic materials for the HER.

Acknowledgements

This work was supported by the National Natural Science Foundation of China (Grant Nos. 51671087 and 11504303); the Foundation for Innovative Research Groups of the National Natural Science Foundation of China (Grant No. 51621001); the Foundation for Research Groups of the Natural Science Foundation of Guangdong Province (Grant No. 2016A030312011) and the Special Support Plan for National 10000-talents Program.

Appendix A. Supplementary data

Supplementary data to this article can be found online at https://doi.org/10.1016/j.ijhydene.2018.10.201.

REFERENCES

[1] Turner JA. Sustainable hydrogen production. Science 2004;305:972–4.
[2] Chu S, Majumdar A. Opportunities and challenges for a sustainable energy future. Nature 2012;488:294–303.
[3] Jiao Y, Zheng Y, Jaroniec M, Qiao SZ. Design of electrocatalysts for oxygen- and hydrogen-involving energy conversion reactions. Chem Soc Rev 2015;44:2060–86.
[4] Shinagawa T, Takanabe K. Towards versatile and sustainable hydrogen production via electrocatalytic water splitting: electrolyte engineering. ChemSusChem 2017;10:1318–36.
[5] Wang CC, Yu Z, Wang XT, Lin B. Enhanced electrocatalytic performance of NiO_x@MnO_x@graphene for oxygen reduction and evolution reactions. Int J Hydrogen Energy 2018;43:18992–9001.
[6] Ding Y, Li H, Hou Y. Phosphorus-doped nickel sulfides/nickel foam as electrode materials for electrocatalytic water splitting. Int J Hydrogen Energy 2018;43:19002–9.
[7] Sheng WC, Gasteiger HA, Shao-Horn Y. Hydrogen oxidation and evolution reaction kinetics on platinum: acid vs alkaline electrolytes. J Electrochem Soc 2010;157:B1529–36.
[8] Carmo M, Fritz DL, Mergel J, Stolten D. A comprehensive review on PEM water electrolysis. Int J Hydrogen Energy 2013;38:4901–34.
[9] Jaramillo TF, Jørgensen KP, Bonde J, Nielsen JH, Horch S, Chorkendorff I. Identification of active edge sites for electrochemical H_2 evolution from MoS_2 nanocatalysts. Science 2007;317:100–2.
[10] Anantharaj S, Ede SR, Sakthikumar K, Karthick K, Mishra S, Kundu S. Recent trends and perspectives in electrochemical water splitting with an emphasis to sulphide, selenide and phosphide catalysts of Fe, Co and Ni: a Review. ACS Catal 2016;6:8069–97.
[11] Wu Y, Li GD, Liu Y, Yang L, Lian X, Asefa T, et al. Overall water splitting catalyzed efficiently by an ultrathin nanosheet-built, hollow Ni_3S_2-based electrocatalyst. Adv Funct Mater 2016;26:4839–47.
[12] Liu Y, Li Q, Si R, Li GD, Li W, Liu DP, et al. Coupling sub-nanometric copper clusters with quasi-amorphous cobalt sulfide yields efficient and robust electrocatalysts for water splitting reaction. Adv Mater 2017;29:1606200.
[13] Shi Y, Zhang B. Recent advances in transition metal phosphide nanomaterials: synthesis and applications in hydrogen evolution reaction. Chem Soc Rev 2016;45:1529–41.
[14] Chung DY, Jun SW, Yoon G, Kim H, Yoo JM, Lee KS, et al. Large-scale synthesis of carbon-shell-coated FeP nanoparticles for robust hydrogen evolution reaction electrocatalyst. J Am Chem Soc 2017;139:6669–74.
[15] Liao L, Wang S, Xiao J, Bian X, Zhang Y, Scanlon MD, et al. A nanoporous molybdenum carbide nanowire as an

electrocatalyst for hydrogen evolution reaction. Energy Environ Sci 2014;7:387–92.
[16] Wang ZL, Hao XF, Jiang Z, Sun XP, Xu D, Wang J, et al. C and N hybrid coordination derived Co-C-N complex as a highly efficient electrocatalyst for hydrogen evolution reaction. J Am Chem Soc 2015;137:15070–3.
[17] Ma FX, Wu HB, Xia BY, Xu CY, Lou XW. Hierarchical β-Mo_2C nanotubes organized by ultrathin nanosheets as a highly efficient electrocatalyst for hydrogen production. Angew Chem Int Ed 2015;54:15395–9.
[18] Cao B, Veith GM, Neuefeind JC, Adzic RR, Khalifah PG. Mixed close-packed cobalt molybdenum nitrides as non-noble metal electrocatalysts for the hydrogen evolution reaction. J Am Chem Soc 2013;135:19186–92.
[19] Zhang B, Xiao C, Xie S, Liang J, Chen X, Tang Y. Iron–nickel nitride nanostructures *in situ* grown on surface-redox etching nickel foam: efficient and ultra-sustainable electrocatalysts for overall water splitting. Chem Mater 2016;28:6934–41.
[20] Tang C, Cheng NY, Pu ZH, Xing W, Sun XP. NiSe nanowire film supported on nickel foam: an efficient and stable 3D bifunctional electrode for full water splitting. Angew Chem Int Ed 2015;54:9351–5.
[21] McCarthy CL, Downes CA, Schueller EC, Abuyen K, Brutchey RL. Method for the solution deposition of phase-pure $CoSe_2$ as an efficient hydrogen evolution reaction electrocatalyst. ACS Energy Lett 2016;1:607–11.
[22] Tong J, Li W, Wei B, Bo L, Li Q, Li Y, et al. Facile preparing composite of $CoSe_2$ wrapping. N-doped mesoporous carbon with highly electrocatalytic activity for hydrogen evolution reaction. Int J Hydrogen Energy 2018;43:17021–9.
[23] Gong M, Zhou W, Tsai MC, Zhou J, Guan M, Lin MC, et al. Nanoscale nickel oxide/nickel heterostructures for active hydrogen evolution electrocatalysis. Nat Commun 2014;5:4695.
[24] Wang H, Lee HW, Deng Y, Lu Z, Hsu PC, Liu Y, et al. Bifunctional non-noble metal oxide nanoparticle electrocatalysts through lithium-induced conversion for overall water splitting. Nat Commun 2015;6:7261.
[25] Luo Z, Miao R, Huan TD, Mosa IM, Poyraz AS, Zhong W, et al. Mesoporous MoO_{3-x} material as an efficient electrocatalyst for hydrogen evolution reactions. Adv Energy Mater 2016;6:1600528.
[26] Zhang PL, Wang M, Yang Y, Yao TY, Han HX, Sun LC. Electroless plated Ni–B_x films as highly active electrocatalysts for hydrogen production from water over a wide pH range. Nanomater Energy 2016;19:98–107.
[27] Li H, Wen P, Li Q, Dun C, Xing J, Lu C, et al. Earth-abundant iron diboride (FeB_2) nanoparticles as highly active bifunctional electrocatalysts for overall water splitting. Adv Energy Mater 2017:1700513.
[28] Xu N, Cao G, Chen Z, Kang Q, Dai H, Wang P. Cobalt nickel boride as an active electrocatalyst for water splitting. J Mater Chem 2017;5:12379–84.
[29] Das RK, Wang Y, Vasilyeva SV, Donoghue E, Pucher I, Kamenov G, et al. Extraordinary hydrogen evolution and oxidation reaction activity from carbon nanotubes and graphitic carbons. ACS Nano 2014;8:8447–56.
[30] Zhuo JQ, Wang TY, Zhang G, Liu L, Gan LB, Li MX. Salts of $C_{60}(OH)_8$ electrodeposited onto a glassy carbon electrode: surprising catalytic performance in the hydrogen evolution reaction. Angew Chem Int Ed 2013;52:10867–70.
[31] Wang J, Cui W, Liu Q, Xing Z, Asiri AM, Sun X. Recent progress in cobalt-based heterogeneous catalysts for electrochemical water splitting. Adv Mater 2016;28:215–30.
[32] Kong D, Wang H, Lu Z, Cui Y. $CoSe_2$ nanoparticles grown on carbon fiber paper: an efficient and stable electrocatalyst for hydrogen evolution reaction. J Am Chem Soc 2014;136:4897–900.
[33] Thomas JM, Raja R, Lewis DW. Single-site heterogeneous catalysts. Angew Chem Int Ed 2005;44:6456–82.
[34] Seh ZW, Kibsgaard J, Dickens CF, Chorkendorff I, Norskov JK, Jaramillo TF. Combining theory and experiment in electrocatalysis: insights into materials design. Science 2017;355:4998.
[35] Staszak-Jirkovský J, Malliakas CD, Lopes PP, Danilovic N, Kota SS, Chang KC, et al. Design of active and stable Co–Mo–S_x chalcogels as pH-universal catalysts for the hydrogen evolution reaction. Nat Mater 2016;15:197–204.
[36] Ma YY, Wu CX, Feng XJ, Tan HQ, Yan LK, Liu Y, et al. Highly efficient hydrogen evolution from seawater by a low-cost and stable CoMoP@C electrocatalyst superior to Pt/C. Energy Environ Sci 2017;10:788–98.
[37] Wu A, Xie Y, Ma H, Tian C, Gu Y, Yan H, et al. Integrating the active OER and HER components as the heterostructures for the efficient overall water splitting. Nanomater Energy 2018;44:353–63.
[38] Cui H, Li B, Zhang Y, Zheng X, Li X, Li Z, et al. Constructing Z-scheme based $CoWO_4$/CdS photocatalysts with enhanced dye degradation and H_2 generation performance. Int J Hydrogen Energy 2018;43:18242–52.
[39] Yu L, Mishra IK, Xie Y, Zhou H, Sun J, Zhou J, et al. Ternary $Ni_{2(1-x)}Mo_{2x}P$ nanowire arrays toward efficient and stable hydrogen evolution electrocatalysis under large-current-density. Nanomater Energy 2018;53:492–500.
[40] Dai ZF, Geng HB, Wang J, Luo YB, Li B, Zong Y, et al. Hexagonal-phase cobalt monophosphosulfide for highly efficient overall water splitting. ACS Nano 2017;11:11031–40.
[41] Danilovic N, Subbaraman R, Strmcnik D, Chang KC, Paulikas AP, Stamenkovic VR, et al. Enhancing the alkaline hydrogen evolution reaction activity through the bifunctionality of $Ni(OH)_2$/metal catalysts. Angew Chem Int Ed 2012;51:12495–8.
[42] Subbaraman R, Tripkovic D, Chang KC, Strmcnik D, Paulikas AP, Hirunsit P, et al. Trends in activity for the water electrolyser reactions on 3d M (Ni, Co, Fe, Mn) hydr(oxy)oxide catalysts. Nat Mater 2012;11:550–7.
[43] Cao GX, Xu N, Chen ZJ, Kang Q, Dai HB, Wang P. Cobalt–tungsten–boron as an active electrocatalyst for water electrolysis. Chemistry 2017;2:6187–93.
[44] Subbaraman R, Tripkovic D, Strmcnik D, Chang KC, Uchimura M, Paulikas AP, et al. Enhancing hydrogen evolution activity in water splitting by tailoring Li^+-$Ni(OH)_2$-Pt interfaces. Science 2011;334:1256–60.
[45] Guinea F. Charge distribution and screening in layered graphene systems. Phys Rev B 2007;75:235433.
[46] Chen HA, Hsin CL, Huang YT, Tang ML, Dhuey S, Cabrini S, et al. Measurement of interlayer screening length of layered graphene by plasmonic nanostructure resonances. J Phys Chem C 2013;117:22211–7.
[47] Deng J, Ren P, Deng D, Bao X. Enhanced electron penetration through an ultrathin graphene layer for highly efficient catalysis of the hydrogen evolution reaction. Angew Chem Int Ed 2015;54:2100–4.
[48] Chen YY, Zhang Y, Zhang X, Tang T, Luo H, Niu S, et al. Self-templated fabrication of $MoNi_4/MoO_{3-x}$ nanorod arrays with dual active components for highly efficient hydrogen evolution. Adv Mater 2017;29:1703311.
[49] Liang HW, Brüller S, Dong RH, Zhang J, Feng XL, Müllen K. Molecular metal-N_x centres in porous carbon for electrocatalytic hydrogen evolution. Nat Commun 2015;6:7992.

[50] Zhang J, Wang T, Liu P, Liu S, Dong R, Zhuang X, et al. Engineering water dissociation sites in MoS_2 nanosheets for accelerated electrocatalytic hydrogen production. Energy Environ Sci 2016;9:2789–93.
[51] Zhang B, Liu J, Wang J, Ruan Y, Jia X, Xu K, et al. Interface engineering: the $Ni(OH)_2/MoS_2$ heterostructure for highly efficient alkaline hydrogen evolution. Nanomater Energy 2017;37:74–80.
[52] Parsons R. The rate of electrolytic hydrogen evolution and the heat of adsorption of hydrogen. Trans Faraday Soc 1958;54:1053–63.
[53] Li H, Tsai C, Koh AL, Cai L, Contryman AW, Fragapane AH, et al. Activating and optimizing MoS_2 basal planes for hydrogen evolution through the formation of strained sulphur vacancies. Nat Mater 2016;15:48–53.
[54] Tsai C, Abild-Pedersen F, Nørskov JK. Tuning the MoS_2 edge-site activity for hydrogen evolution *via* support interactions. Nano Lett 2014;14:1381–7.
[55] Zhang J, Wang T, Liu P, Liao Z, Liu S, Zhuang X, et al. Efficient hydrogen production on $MoNi_4$ electrocatalysts with fast water dissociation kinetics. Nat Commun 2017;8:15437.